ECCOMAS Congress 2016
VII European Congress on Computational Methods in Applied Sciences and Engineering
M. Papadrakakis, V. Papadopoulos, G. Stefanou, V. Plevris (eds.)
Crete Island, Greece, 5–10 June 2016

A cell-based smoothed point interpolation method for axisymmetric problems

A. Tootoonchi[*] and A. Khoshghalb[*]

* School of Civil and Environmental Engineering, UNSW Australia, Sydney, NSW, 2052, Australia

KEY WORDS: axisymmetric, meshfree methods, smoothing gradient operation, saturated porous media, point interpolation method.

Abstract. *A cell-based smoothed point interpolation method (CSPIM) for the numerical modelling of saturated porous media in axisymmetric conditions is proposed. Spatial discretisation is performed using a simple triangulation. Both displacement and fluid pressure gradients are smoothed by incorporating the smoothing gradient operation technique. Thus, the integration over the supporting domains (i.e. elements) is transformed to that over the boundary of the elements. The field variables, the displacement and excess pore water pressure, are interpolated using point interpolation shape functions (polynomial and radial), which possess the Kronecker function property and facilitate imposing the essential boundary conditions. The global property matrices of the discretised system of equations are derived using the generalised smoothed Galerkin method and the three-point time discretisation scheme for discretisation of the governing equations in space and time, respectively. A novel approach is introduced for the computation of the property matrices, which avoids the singularity problem that will otherwise arise when cell-based smoothed interpolation method is used in axisymmetric conditions. The salient feature of the proposed method is that it incurs no additional computational costs, and it does not compromise on accuracy of the method. The validity of the proposed method is investigated by simulation of Cryer's benchmark consolidation problem. The numerical results are in excellent agreement with the analytical solution.*

Introduction

A wide class of efficient smoothed point interpolation methods (SPIMs) have been recently developed [1, 2] by incorporating strain smoothing operation [2] to point interpolation methods (PIMs). In SPIMs, instead of using a compatible strain field, a smoothed strain field is constructed through a smoothing operation performed over smoothing domains. The smoothed strain field overcomes the problems associated with continuity of the approximation field over the problem domain through elimination of the need for the derivatives of the shape functions. Different smoothing domains can be adopted for the smoothing operation leading to different SPIMs [3-6]. The simplest SPIM is perhaps the cell-based SPIM (CSPIM) in which the cells of a triangular background mesh are used as the smoothing domains. To date, CSPIM has been successfully applied to plane strain problems in geotechnical engineering with results showing its superiority to similar methods (e.g. finite element methods) in terms of both efficiency and convergence rate [7].

Axisymmetric problems are of considerable importance in geotechnical engineering because of their many applications including simulation of uni-axial and tri-axial loading conditions, pile installation, and tunnels. Nonetheless, application of SPIMs to axisymmetric problems has received little attention in the literature. This may be attributed to the difficulties associated with application of SPIMs in axisymmetric conditions due to the existence of Gauss points on the boundary of the smoothing domains on the axis of the symmetry. In particular, CSPIM cannot be directly extended to axisymmetric conditions due to singularity problem arises in the analysis.

In this paper, a novel approach is presented to extend the formulation of the CSPIM to axisymmetric conditions. The approach is general in nature and can also be applied to other SPIMs to extend their application to axisymmetric problems. The technique presented does not include any approximation and therefore, does not adversely affect the accuracy of the numerical procedure. The validity of the proposed method is verified by analysis of Cryer's benchmark problem [8].

Governing equations

The equations governing flow-deformation of saturated porous media, first presented by Biot [9], are derived based on the momentum balance of the solid and fluid phases and mass conservation of the fluid phase, as

$$\boldsymbol{\partial}^T\left[\boldsymbol{D}\dot{\boldsymbol{\varepsilon}} + \eta\dot{\tilde{p}}_f\boldsymbol{\delta}\right] + \dot{\boldsymbol{F}} = \boldsymbol{0} \tag{1}$$

$$\boldsymbol{\nabla}^T\left(\frac{\boldsymbol{k}_f}{\mu_f}\left(\boldsymbol{\nabla}\tilde{p}_f + \rho_f\boldsymbol{g}\right)\right) = a_f\dot{\tilde{p}}_f - \boldsymbol{\nabla}^T\dot{\tilde{\boldsymbol{u}}} \tag{2}$$

with

$$a_f = n\left(c_f - c_s\right) + \eta c_s \quad , \quad \eta = 1 - \frac{c_s}{c} \tag{3}$$

where $\boldsymbol{D}$ is the drained stiffness matrix of the soil, $\boldsymbol{\varepsilon}$ is the soil skeleton strain, $\boldsymbol{\delta}$ is the Kronecker delta, $\boldsymbol{F}$ is the vector of body force per unit volume, a_f is the apparent compressibility of the fluid, c_f is the compressibility of the fluid, c_s is the compressibility of solid grains, c is the drained compressibility of the solid skeleton and η is the effective stress parameter. $\boldsymbol{k}_f$ is the intrinsic permeability matrix of the soil, μ_f is the dynamic viscosity of the fluid and ρ_f is the intrinsic mass densities of the fluid. $\tilde{\boldsymbol{u}}$ stands for the displacement vector of the soil skeleton and $\tilde{p}_f$ is the pore fluid pressure (the tilde denotes a continuous field as opposed to the discretised field introduced later). $\boldsymbol{g}$ is the vector of gravitational acceleration and n is the soil porosity. $\boldsymbol{\partial}$ and $\boldsymbol{\nabla}$ are the differentiation matrix and the gradient operator, respectively.

Construction of the shape functions

Radial Point Interpolation Method (RPIM) [10] is adopted in this study for the construction of the nodal shape functions. To derive RPIM shape functions, the field approximation function, $u(\boldsymbol{x})$, in the space coordinates $\boldsymbol{x}$=$[r, z]$ is approximated at any point in the problem domain with the following series representation:

$$u(\boldsymbol{x}) = \sum_{i=1}^{p} a_i R_i(\boldsymbol{x}) + \sum_{j=1}^{l} b_j p_j(\boldsymbol{x}) = \boldsymbol{R}^T(\boldsymbol{x})\boldsymbol{a} + \boldsymbol{p}^T(\boldsymbol{x})\boldsymbol{b} \tag{4}$$

in which $R_i(\boldsymbol{x})$ and $p_j(\boldsymbol{x})$ are the radial basis functions (RBFs) and monomial terms, respectively; a_i is the coefficient for radial basis $R_i(\boldsymbol{x})$, and b_j is the coefficient for the polynomial basis $p_j(\boldsymbol{x})$. p is the number of nodes in the compact support domain of the point of interest, and j is the number of monomial terms. Detailed discerption of derivation of shape functions can be found in previous works [10-14].

Cell-based smoothed strains

In CSPIM, the cells of the background mesh serve as the smoothing domains, with the smoothed strains computed for each cell through the smoothing operation technique. The smoothed strain for cell k can be calculated from [2],

$$\hat{\boldsymbol{\varepsilon}}_k = \hat{\boldsymbol{B}}_1 \boldsymbol{u} = \frac{1}{\Omega^k}\int_{\Omega^k} \boldsymbol{\nabla} u(\boldsymbol{x}) d\Omega^k = \frac{1}{\Omega^k}\int_{\Gamma^k} \boldsymbol{L}_n u(\boldsymbol{x}) d\Gamma^k \tag{5}$$

where $\hat{\boldsymbol{B}}_1$ is the smoothed strain-displacement matrix for each smoothing domain, which is obtained by the summation of the smoothed strain-displacement matrices computed at the Gauss points on the edges of the smoothing domain, as follows:

$$\hat{\boldsymbol{\varepsilon}}_k = \sum_{i=1}^{q} \hat{\boldsymbol{B}}_{1i} \boldsymbol{u}_i \qquad\qquad i \in S_s \tag{6}$$

where S_s is the set of q support nodes that includes all the nodes involved in the interpolation of the quadrature points located on all segments of the boundary Γ^k for the smoothing domain Ω^k. $\boldsymbol{L}_n$ in equation (6) is unit outward operator for each segment of the boundary of cell k. Further details about the computation of the smoothed strain-displacement matrix can be found in [7].

Node selection schemes

In CSPIM, a number of node selection schemes, known as T-schemes, have been proposed for the selection of the supporting nodes at each point of interest. Comprehensive details of the T-Schemes can be found in Liu and Zhang [2]. In the current study, a simple node selection scheme, referred to as T4, is adopted. This scheme selects four nodes of the two cells that share the edge hosting the Gauss point of interest. A linear approximation is applied when the Gauss point of interest is located on the boundary of the domain.

Spatial and temporal discretisations

Using the Generalised Smoothed Galerkin (GS Galerkin) approach [2], the spatial discretisation of equations (1) and (2) are obtained as follows [7]:

$$\widehat{\boldsymbol{E}}\boldsymbol{U} + \varrho\widehat{\boldsymbol{C}}\boldsymbol{P}_f = \boldsymbol{R} \tag{7}$$

$$\varrho\widehat{\boldsymbol{C}}^T\dot{\boldsymbol{U}} - \widehat{\boldsymbol{H}}\boldsymbol{P}_f - a_f\boldsymbol{M}\dot{\boldsymbol{P}}_f = \boldsymbol{Q} \tag{8}$$

The smoothed-displacement matrix for an axisymmetric setting is as follows

$$\widehat{\boldsymbol{B}}_1 = \sum_{i\in S_s}\widehat{\boldsymbol{B}}_{1i} = \sum_{i\in S_s}\begin{bmatrix}\hat{b}_{ir} & 0\\ 0 & \hat{b}_{iz}\\ \hat{b}_{iz} & \hat{b}_{ir}\\ \frac{\phi_i}{r} & 0\end{bmatrix} \tag{9}$$

where

$$\hat{b}_{il} = \frac{1}{2\Omega^k}\sum_{\mathrm{m}=1}^{N_{seg}}\left[L_m^k\sum_{\mathrm{n}=1}^{N_{gau}} w_n\,\phi_i(\boldsymbol{x}_{mn})\;n_l(\boldsymbol{x}_{mn})\right]\quad (l=r,z) \tag{10}$$

where N_{seg} is the number of line segments, L_m^k is the length of the mth segment of Γ^k, n_l is the component of the unit outward normal and N_{gau} is the number of Gauss points used in each segment of Γ^k, which is taken two in this study. $\boldsymbol{x}_{mn}$ is the nth Gauss point of the mth segment of Γ^k, and w_n is the Gauss integration weight. $\phi_i(\boldsymbol{x}_{mn})$ is the shape function value for node $i \in S_s$ at the point of interest $\boldsymbol{x}_{mn}$. If the current quadrature point $i \notin S_n$, then $\phi_i(\boldsymbol{x}_{mn}) = 0$.

As can be seen, the term ϕ_i/r in equation (9) leads to a singularity problem when the Gauss point of interest is on the axis of symmetry. To overcome this problem, the smoothed strain-displacement matrix is decomposed into two matrices:

$$\widehat{\boldsymbol{B}}_1 = \widehat{\boldsymbol{B}}_{1s} + \boldsymbol{B}_{1\Theta} \tag{11}$$

where

$$\widehat{\boldsymbol{B}}_{1s} = \sum_{i\in S_s} \widehat{\boldsymbol{B}}_{1si} = \sum_{i\in S_s} \begin{bmatrix} \hat{b}_{ir} & 0 \\ 0 & \hat{b}_{iz} \\ \hat{b}_{iz} & \hat{b}_{ir} \\ 0 & 0 \end{bmatrix} \tag{12}$$

$$\boldsymbol{B}_{1\theta} = \sum_{i\in S_s} \boldsymbol{B}_{1\theta i} = \sum_{i\in S_s} \begin{bmatrix} 0 & 0 \\ 0 & 0 \\ 0 & 0 \\ \frac{\phi_i}{r} & 0 \end{bmatrix} \tag{13}$$

The decomposition separates the terms causing singularity from the rest of the strain-displacement matrix. Given that no smoothing is required for ϕ_i/r terms, the integrations involving this term can be carried out over the smoothing domains rather than the boundary of the smoothing domains, resulting in the removal of the singularity problem. The procedure involves no additional computational cost as in any case, the shape function values are calculated at the Gauss points inside the smoothing domains for the calculation of $\boldsymbol{M}$ and $\widehat{\boldsymbol{C}}$, even in plane strain problems [7]. For the stiffness matrix,

$$\widehat{\boldsymbol{E}} = \sum_{k=1}^{N_{SD}} 2\pi r\left(\widehat{\boldsymbol{B}}_{1s}^T \boldsymbol{D} \widehat{\boldsymbol{B}}_{1s} + \widehat{\boldsymbol{B}}_{1s}^T \boldsymbol{D} \widehat{\boldsymbol{B}}_{1\theta} + \widehat{\boldsymbol{B}}_{1\theta}^T \boldsymbol{D} \widehat{\boldsymbol{B}}_{1s} + \widehat{\boldsymbol{B}}_{1\theta}^T \boldsymbol{D} \widehat{\boldsymbol{B}}_{1\theta}\right)\Omega^k \tag{14}$$

The first term in equation (14) is calculated similar to the computation of the stiffness matrix in CSPIM of plane strain problems [9]. The second and third terms are calculated adopting an approach similar to that proposed in [1] for the calculation of the $\widehat{\boldsymbol{C}}$ matrix. The last term is calculated over the smoothing domains using the standard Gauss integration approach.

The coupling matrix is calculated as follows

$$\widehat{\boldsymbol{C}} = \sum_{k=1}^{N_{\mathrm{SD}}} \widehat{\boldsymbol{C}}^{SD} = \sum_{k=1}^{N_{\mathrm{SD}}} 2\pi \left(\int_{\Omega^k} (\widehat{\boldsymbol{B}}_{2s} + \boldsymbol{B}_{2\Theta})^T \boldsymbol{\Phi}^p r \, d\Omega^k\right) \tag{15}$$

where $\boldsymbol{\Phi}^p$ is the matrix of shape functions. The first part of the integration is calculated similar to the $\widehat{\boldsymbol{C}}$ matrix in plain strain formulation [7]. The second term is obtained over the smoothing domain using the standard Gauss integration approach.

The Permeability matrix ($\widehat{\boldsymbol{H}}$) and the compressibility matrix of the fluid phase ($\boldsymbol{M}$) can be computed with small modifications to the formulations presented in [7], as follows

$$\widehat{\boldsymbol{H}} = \sum_{k=1}^{N_{\mathrm{SD}}} \widehat{\boldsymbol{H}}^{SD} = \sum_{k=1}^{N_{\mathrm{SD}}} \frac{2\pi}{\mu_f} \widehat{\boldsymbol{B}}_3^T \boldsymbol{k}_f \widehat{\boldsymbol{B}}_3 \int_{\Omega^k} r \, d\Omega^k \tag{16}$$

$$\boldsymbol{M} = \sum_{k=1}^{N_{\mathrm{SD}}} \boldsymbol{M}^{SD} = \sum_{k=1}^{N_{\mathrm{SD}}} 2\pi \int_{\Omega^k} \boldsymbol{\Phi}^{pT} \boldsymbol{\Phi}^p r d\Omega^k \tag{17}$$

Equations (7) and (8) are then discretised in time using a three point time discretisation scheme [15] resulting in the fully discretised systems of equations, as follows

$$\boldsymbol{K}\boldsymbol{W} = \boldsymbol{Y} \tag{18}$$

$$\boldsymbol{K} = \begin{bmatrix} A\widehat{\boldsymbol{E}}_{2N\times 2N} & A\varrho\widehat{\boldsymbol{C}}_{2N\times N} \\ A\varrho\widehat{\boldsymbol{C}}^{\boldsymbol{T}}{}_{N\times 2N} & -\left(\Delta t\widehat{\boldsymbol{H}} + Aa_f\boldsymbol{M}\right)_{N\times N} \end{bmatrix}_{3N\times 3N} \tag{19}$$

$$\boldsymbol{W} = \begin{bmatrix} \boldsymbol{U}^{t+\alpha\Delta t}{}_{2N\times 1} \\ \boldsymbol{P}_f^{t+\alpha\Delta t}{}_{N\times 1} \end{bmatrix}_{3N\times 1} \tag{20}$$

$$\boldsymbol{Y} = \begin{bmatrix} A(\boldsymbol{R}^{t+\alpha\Delta t})_{2N\times 1} \\ (\Delta t\boldsymbol{Q}^{t+\alpha\Delta t} + B\varrho\widehat{\boldsymbol{C}}^T\boldsymbol{U}^t - C\varrho\widehat{\boldsymbol{C}}^T\boldsymbol{U}^{t-\Delta t} - Ba_f\boldsymbol{M}\boldsymbol{P}_f^t + Ca_f\boldsymbol{M}\boldsymbol{P}_f^{t-\Delta t})_{N\times 1} \end{bmatrix}_{3N\times 1} \tag{21}$$

Verification

The benchmark consolidation problem of Cryer is adopted here for verification purposes. In this problem, a uniformly distributed surface load of $p_0 = 1\ kPa$ is concentrically applied to a sphere of radius $a = 1.0\ m$. Only a quarter of the sphere was modelled, because of the symmetry. The outer boundary of the sphere was assumed permeable and the permeability of the sphere was assumed $k = 1\ m/s$. The geometry and boundary conditions of the problem, along with the triangular background mesh used for the spatial discretisation are shown in Figure 1. Three different cases were studied using three different sets of elastic properties as presented in Table 1. Case 3 here approximates an incompressible material (ν = 0.5). In all cases, the first dimensionless time step was taken as 0.0005 with a time step growth factor of 1.2.

Table 1. Soil properties used in the analysis of Cryer's problem

Case Number	*ν*	*E*
1	0.0	1.0
2	0.333	0.666
3	0.496	0.0299

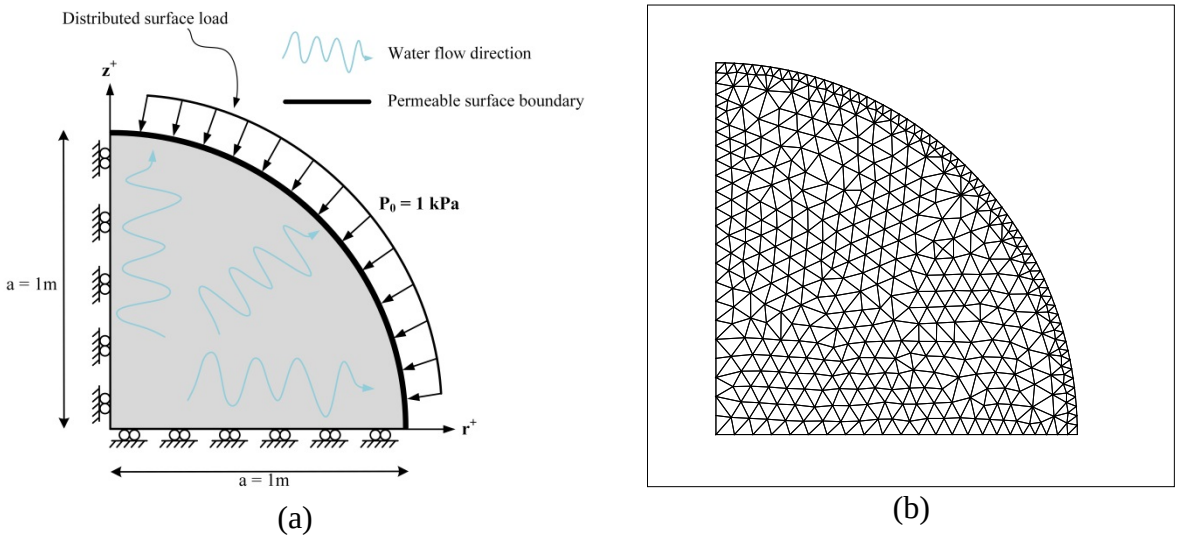

Figure 1. consolidation problem of Cryer; a) Geometry and boundary conditions; b) Spatial discretisation used in this study

As an example, the numerical results for the excess pore water pressure contours from the analysis of case 1 at dimensionless time 0.01979 is shown in Figure 2. The symmetry of the geometry and the applied load result in the symmetry of the excess pore water pressure contour, as expected.

The analytical solution for the excess pore water pressure generated at the centre of the sphere versus dimensionless radial displacement of the surface of the sphere, and also the variation of the dimensionless surface settlement with time were derived by Cryer [8]. For the verification of the proposed formulation, the results of the numerical analysis are compared with the analytical solution as presented in Figure 3. As can be seen, there is an excellent agreement between the results of the proposed method and the analytical solution for all three cases studied. In all cases, the pore pressure increases over the entire sphere to the value of the applied load upon the application of the load. The pore pressure then initially increases at the centre of the sphere in cases 1 and 2, before decreasing due to consolidation process. This effect, known as the Mandel-Cryer effect [8, 16], is perfectly captured in the numerical analyses. For case 3, when the soil is incompressible, no increase of pore water pressure is observed which also agrees with the analytical solution. The Mandle-Cryer effect cannot be captured using the original Terzaghi's formulation for consolidation and can only be simulated when the governing equations for the solid and water phases are properly coupled. More discussion on this matter can be found in [17].

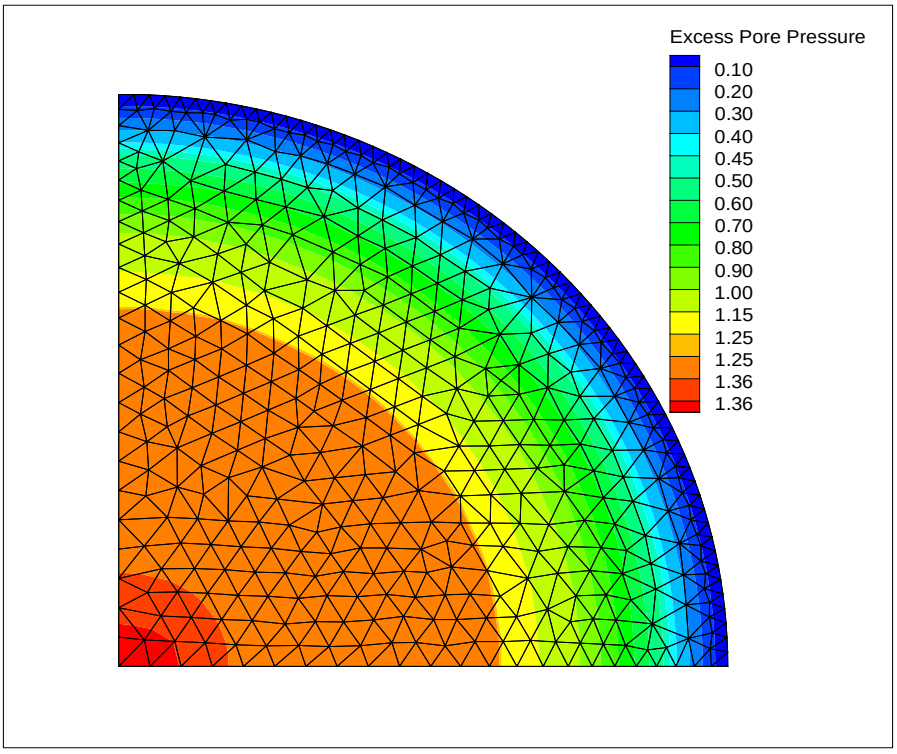

Figure 2. Excess pore pressure contour for Cryer's problem at dimensionless time of 0.01979.

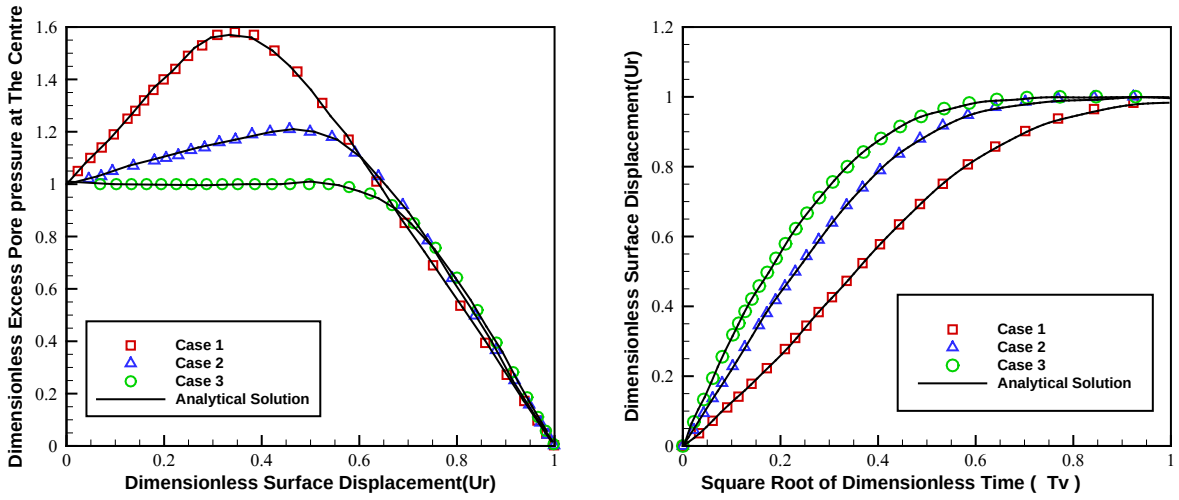

Figure 3. Comparison between numerical results and analytical solution; (a) Dimensionless excess pore pressure at the centre of the sphere versus dimensionless surface displacement; (b) dimensionless surface displacement versus $\sqrt{T_v}$

Conclusion

A cell-based smoothed point interpolation method (CSPIM) for the analyses of axisymmetric poro-elastic problems has been proposed. This method is based on a novel approach for systematic decomposition of the system matrices to remove the inherent singularity problem in SPIMs when an axisymmetric problem is considered. Solid and fluid phase property matrices and coupling matrices of a fully discretised system of equations have been derived in an axisymmetric setting based on the proposed approach. The method has been verified by numerical analysis of Cryer's benchmark problem of consolidation of a saturated sphere. It has been shown that the proposed method can accurately reproduce the analytical solution and in particular, the Mandel-Cryer effect is precisely captured when a compressible medium is considered.

References

1. Liu, G., G. Zhang, K. Dai, Y. Wang, Z. Zhong, G. Li, and X. Han, *A linearly conforming point interpolation method (LC-PIM) for 2D solid mechanics problems.* International Journal of Computational Methods, 2005. **2**(04): p. 645-665.
2. Liu, G.-R. and G.-Y. Zhang, *Smoothed point interpolation methods: G space theory and weakened weakforms*. 2013.
3. Cui, X., G. Liu, G. Li, X. Zhao, T. Nguyen-Thoi, and G. Sun, *A smoothed finite element method (SFEM) for linear and geometrically nonlinear analysis of plates and shells.* Comput Model Eng Sci, 2008. **28**(2): p. 109-125.
4. Liu, G. and G. Zhang, *Edge-based smoothed point interpolation methods.* International Journal of Computational Methods, 2008. **5**(04): p. 621-646.
5. Liu, G. and G. Zhang, *A normed G space and weakened weak (W2) formulation of a cell-based smoothed point interpolation method.* International Journal of Computational Methods, 2009. **6**(01): p. 147-179.

6. Liu, G. and G. Zhang, *Upper bound solution to elasticity problems: A unique property of the linearly conforming point interpolation method (LC-PIM).* International Journal for Numerical Methods in Engineering, 2008. **74**(7): p. 1128-1161.
7. Tootoonchi, A., A. Khoshghalb, G. Liu, and N. Khalili, *A cell-based smoothed point interpolation method for flow-deformation analysis of saturated porous media.* Computers and Geotechnics, 2016. **75**: p. 159-173.
8. Cryer, C., *A comparison of the three-dimensional consolidation theories of Biot and Terzaghi.* The Quarterly Journal of Mechanics and Applied Mathematics, 1963. **16**(4): p. 401-412.
9. Biot, M.A., *General theory of three-dimensional consolidation.* Journal of applied physics, 1941. **12**(2): p. 155-164.
10. Wang, J. and G. Liu, *A point interpolation meshless method based on radial basis functions.* International Journal for Numerical Methods in Engineering, 2002. **54**(11): p. 1623-1648.
11. Liu, G.-R., *Meshfree methods: moving beyond the finite element method*. 2010: CRC press.
12. Liu, G.-R. and Y. Gu, *A point interpolation method for two-dimensional solids.* International Journal for Numerical Methods in Engineering, 2001. **50**(4): p. 937-951.
13. Wang, J. and G. Liu, *On the optimal shape parameters of radial basis functions used for 2-D meshless methods.* Computer methods in applied mechanics and engineering, 2002. **191**(23): p. 2611-2630.
14. Khoshghalb, A. and N. Khalili, *A stable meshfree method for fully coupled flow-deformation analysis of saturated porous media.* Computers and Geotechnics, 2010. **37**(6): p. 789-795.
15. Khoshghalb, A., N. Khalili, and A. Selvadurai, *A three-point time discretization technique for parabolic partial differential equations.* International Journal for Numerical and Analytical Methods in Geomechanics, 2011. **35**(3): p. 406-418.
16. Mandel, J., *Consolidation des sols (étude mathématique)*.* Geotechnique, 1953. **3**(7): p. 287-299.
17. Gibson, R., R. Schiffman, and S. Pu, *Plane strain and axially symmetric consolidation of a clay layer on a smooth impervious base.* The Quarterly Journal of Mechanics and Applied Mathematics, 1970. **23**(4): p. 505-520.